THE JOURNAL OF
PHYSICAL CHEMISTRY C

Article

Cite This: *J. Phys. Chem. C* 2019, 123, 27770−27777

pubs.acs.org/JPCC

Plasmonic Electricity: Fluorophore-Induced Plasmonic Current

Joshua Moskowitz and Chris D. Geddes*

Institute of Fluorescence and Department of Chemistry and Biochemistry, University of Maryland Baltimore County, Baltimore, Maryland 21202, United States

Supporting Information

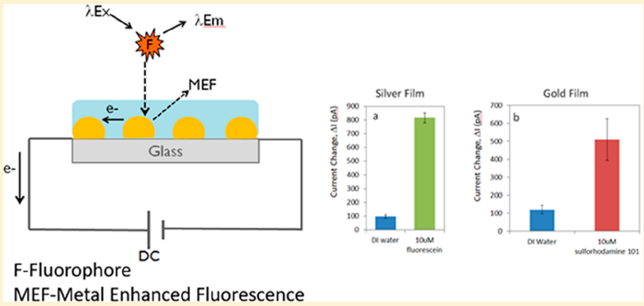

ABSTRACT: Fluorophore-induced plasmonic current is generated when an excited fluorophore in close proximity to a metal nanoparticle film nonradiatively transfers energy to the metal, resulting in an electrical current across the film. Although a growing literature reports the use of surface plasmons for fluorescence enhancement as well as plasmons for current generation, little has been published hitherto regarding the electrical current generation via the fluorophore excitation of plasmons. Our "plasmon to current" technique utilizes electron transport between closely spaced metal nanoparticles, generating a measurable electrical signal upon excitation of a proximal fluorophore. This induced electrical signal is found to be strongly dependent on the magnitude of the fluorophore extinction coefficient. In other words the electrical signal contains photophysical information pertaining to the fluorophore, potentially leading to the direct detection of fluorescence without the need for traditional detectors such as photomultiplier tubes and charge coupled devices. In addition, we demonstrate the dependence of this current on fluorophore concentration and excitation laser polarization. Fluorophore-induced plasmonic current holds potential as a novel molecular detection platform with simplified instrumentation, compatible with a variety of fluorescent probes.

INTRODUCTION

Fluorescence methodologies are entrenched in scientific laboratories today. These methodologies are important for a wide range of applications from single molecule studies to disease diagnosis. In all of these methodologies an optically excited fluorophore emits light which is then detected in the far-field by a photodetector, where the signal is digitally converted and output to a display device. In addition, fluorophores in the near-electric field of metallic nanostructures are known to couple with and transfer energy to the metal, leading to plasmon resonance. Plasmon excitation may then relax in several ways, including the emission of light from the metal itself, at a frequency characteristic of the fluorophore.[1−8]

Fluorescence enhancement in the presence of metallic nanoparticles, known as metal-enhanced fluorescence (MEF), is well studied in the literature and in particular by our group over the last ten years. The metal can use its relatively large size to act as a nanoantenna for the fluorophore, effectively increasing the absorption cross section of the fluorophore.[8−10] Following this absorption, energy transfer may take place from the fluorophore to the metal, where the fluorophore creates a mirror dipole in the metal itself. Here, strong energy transfer is expected when the emission from the fluorophore overlaps with the absorption of the metal,[4] where the enhanced fluorescence emission profile can readily be measured using the synchronous scattering spectrum.[1] The relatively short relaxation lifetime of the plasmon (picoseconds as compared to nanoseconds for fluorophores) is thought to favor the increased radiative rate of the coupled system as compared to the free-space fluorophore itself, increasing the fluorescence intensity.[1] It is well-known that large nanoparticles are required for visible wavelength light MEF,[2] therefore, an enhanced self-absorption inherent with small nanoparticles can be neglected.

Plasmon excitation is increasingly being utilized for the development of a variety of techniques, which use photodetectors such as photomultiplier tubes and charge coupled devices to measure light following plasmon excitation. This light may be internally reflected from a thin metal film at a critical angle, leading to surface plasmon resonance and providing information regarding the refractive index of the surface.[1,11−14] Plasmon resonance is also used for the enhancement of Raman scattering, known as surface enhanced Raman spectroscopy (SERS), which can increase the sensitivity in molecular detection.[11,15,16] In Near-Field Scanning Optical Microscopy, light is scattered from a metal nanoparticle tip due to plasmon resonance, breaking the standard diffraction limit of light microscopy.[17,18] In metal enhanced fluorescence (MEF), a near-field excited fluorophore nonradiatively transfers energy to the metal, and subsequently, the light is emitted from the metal nanoparticles, altering the free space fluorophore emission properties.[1−8] These techniques mentioned above rely on direct detection of the far-field electromagnetic radiation, following plasmon excitation, in

Received: August 29, 2019
Revised: October 21, 2019
Published: October 23, 2019

DOI: 10.1021/acs.jpcc.9b08249
J. Phys. Chem. C 2019, 123, 27770−27777

order to obtain molecular information. In other words, they are "plasmon to light" techniques.

"Plasmon to current" techniques also exist, which utilize plasmon resonance for direct electrical current generation in a semiconductor, providing information regarding both the excitation light frequency and metal plasmon resonance frequency.[19,20] Excitation of a quantum dot leading to the induction of plasmon resonance is also used for electrical current generation, allowing for detection of the quantum dot.[20]

This paper subsequently describes a novel "plasmon to current" technique, potentially capable of molecular detection, alleviating the need for complex and often expensive traditional photodetectors and associated optics. Research in the area of MEF has to lead to our finding that upon energy transfer from a molecular dipole to closely spaced surface metallic nanoparticles, a detectable electrical current may be generated across the surface. This is thought possible because of the close spacing between separate metal nanoparticle islands, allowing for electron transport, also known in the literature as electron "hopping" or "tunnelling" (Figure 1).[21−25]

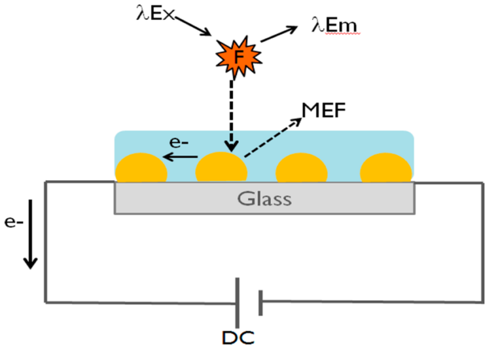

Figure 1. Schematic depicting nonradiative energy transfer from a fluorophore to metal nanoparticle islands, and electron transport between particles. The blue coloring represents a liquid solvent. Electrodes are in simultaneous contact with the metal film and solvent.

Electron transport or "hopping" occurs between metal nanoparticles when the charging energy required for a metal particle to gain an electron is less than the thermal energy of the system, i.e.

$$E_C = \frac{e^2}{2C} < k_B T \tag{1}$$

where E_C is charging energy, e is the elementary electric charge, and C is capacitance of the particle.[21−24] The simple sphere model describes the dependence of capacitance on metal particle size and the relative permittivity of the medium surrounding the particle, where,

$$C = 2\pi\varepsilon_0\varepsilon d \tag{2}$$

where ε_0 is the vacuum permittivity, ε is the relative permittivity of the medium surrounding the particle, and d is the diameter of the spherical particle.[22,24] In addition, it has been demonstrated experimentally that the charging energy of individual particles is decreased as adjacent particles become larger and more closely spaced.[24,25] In other words, holding the temperature and applied voltage constant, as metal particle islands grow larger and more closely spaced, a lower columbic gap to electron "hopping" exists. Metal nanoparticles in our films are surrounded by neighboring nanoparticles (Figure 2a), allowing for use of the concentric sphere model to estimate the capacitance of individual metal nanoparticles in the film, which is a commonly used approach throughout the literature,[24,26−29] where

$$C = 4\pi\varepsilon_0\varepsilon r_0(r_0 + s)/s \tag{3}$$

where r_0 is the particle radius and s is the distance between two neighboring particles.

Placing a liquid such as water between these metal particles increases the relative permittivity in eqs 2 and 3 as compared to air. This increase in relative permittivity decreases the charging energy according to eq 1, favoring increased electron transport in solvent covered metal-nanoparticle films as compared to the dry films. Upon excitation of a proximal fluorophore, energy is transferred from the molecular dipole to the plasmon electrons, a similar mechanism as thought for MEF. This energy is expected to help overcome the columbic gap, increasing electron transport between separate metal-islands, leading to an increased charge transport across the film, and an observed electrical current increase upon fluorophore excitation. Conversely, if large particle spaces and/or a low permeability solvent are used, a decreased current flows, and our ongoing studies suggest MEF is more favorable under these conditions. Subsequently, our findings suggest a way of controlling for either MEF or plasmonic current.

In this paper we report fluorophore-induced electrical current generation between separate metal nanoparticle islands. In addition, we demonstrate the dependence of this current on fluorophore extinction coefficient. This finding suggests the potential for fluorescence to be detected "electrically" without the need for a photodetector. This further suggests new formats for fluorescence instrumentation and sensing platforms, such as for the realization of novel plasmon based immunoassays.

■ RESULTS AND DISCUSSION

Silver-island films were fabricated with either thermal vapor deposition or liquid synthesis using a Tollens reaction. Representative scanning electron microscopy images of silver and gold-island films prepared via thermal vapor deposition are shown in Figure 2a,b, respectively. The silver particles appear as individual spherical islands approximately 40 nm in diameter. The gold particles also appear as individual islands. However, these particles are less spherical compared to the silver particles with a greater range of island geometries. This increased range of island geometries is expected to result in a broadened absorption spectrum for the gold film as compared to silver. Absorption spectrum for silver and gold island films prepared over a range of thermal vapor deposition times are shown in Supporting Information, Figure S1. As the vapor deposition time increases, red-shifted and broadened absorption spectrum are observed, indicating and confirming the growing of the average particle size in the films.[4] intuitively, it is expected that as these sizes grow, the spacing between particles decreases. This is supported by a transformation from noncontinuous (zero measurable current), to low resistance continuous metal films. In other words, the particles grow into each other, decreasing the size of the spaces between the particles. Control and characterization of particle sizes in silver-island films prepared via the liquid Tollens synthesis were obtained in a manner similar to previous work by our

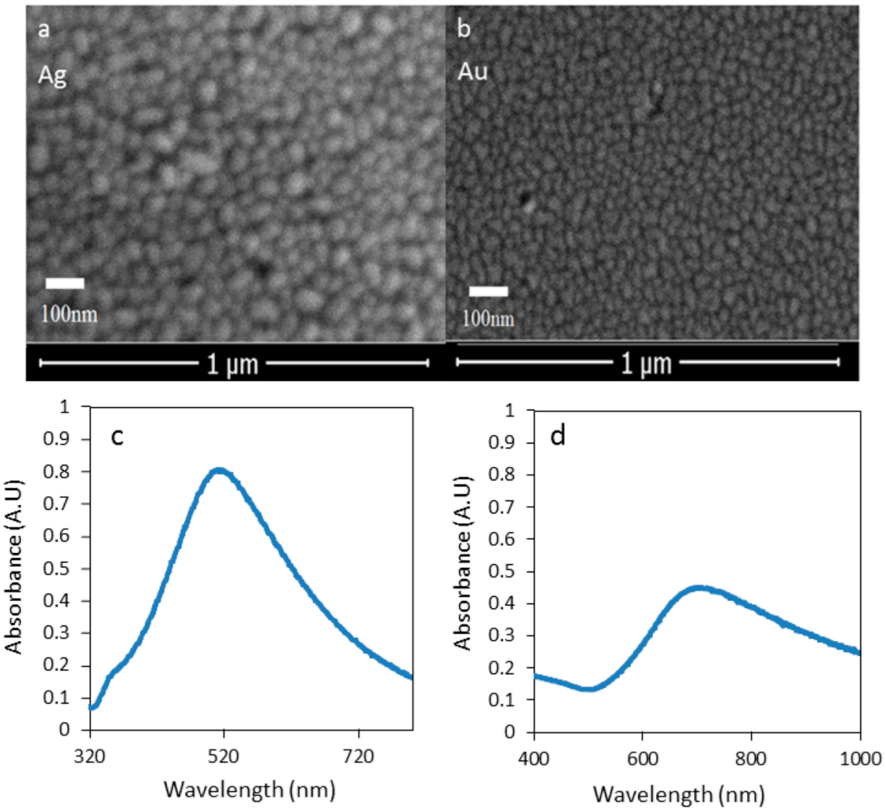

Figure 2. SEM images and corresponding absorption spectra of silver (a,c) and gold (b,d) nanoparticle island films fabricated by thermal vapor deposition.

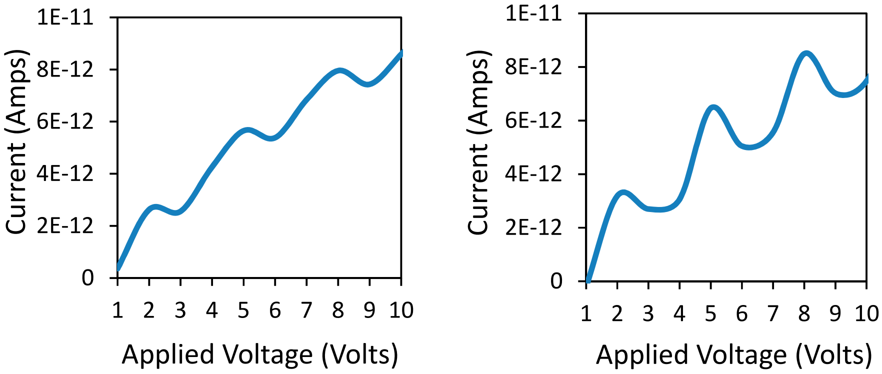

Figure 3. $I-V$ curves for silver (left) and gold (right) nanoparticle island films.

laboratory and elsewhere in the literature.[30−32] Electrical current measurements across a 1 cm portion of each film in an open circuit configuration confirmed the films to be electrically noncontinuous when dry.

Applying the concentric sphere model (eq 3), the capacitance for a 40 nm spherical silver particle with a 2 nm air gap separating its neighboring particles is calculated to be 2.46×10^{-17} F. This is the capacitance of a single particle in the film. However, an estimation for the capacitance between two distant points in the film (for example, between the two electrodes) can be calculated by treating the metal nanoparticle film as a grid containing a large number of identical capacitors. Asad et al. have previously derived an equation for the capacitance between two points on a large grid,[33] which may be applied here to estimate the total capacitance across the nanoparticle film, where

$$\frac{C_{m,n}}{C} = \frac{\pi}{2\ln(m^2 + n^2) + 4\ln \pi + 0.22} \qquad (4)$$

where C is the capacitance of a single nanoparticle and $C_{m,n}$ is the capacitance between two nanoparticles on opposite sides of the nanoparticle film and (m,n) are coordinates on the grid of nanoparticles where an electron enters the grid at (0,0) and exits at (m,n) (Supporting Information, Figure S2). The distance between the two electrodes is 1 cm, which is used to determine the number of particles in a straight line across the film, which is calculated to be $\sim 2.38 \times 10^5$ particles. This value is used for m in eq 4, and n is taken to be zero, in order to determine the capacitance between two points across the film. Taking the capacitance of a single nanoparticle in the film to be 2.46×10^{-17} F, as determined by the concentric sphere model, $C_{m,n}$ is then calculated to be 1.42×10^{-18} F. This leads to

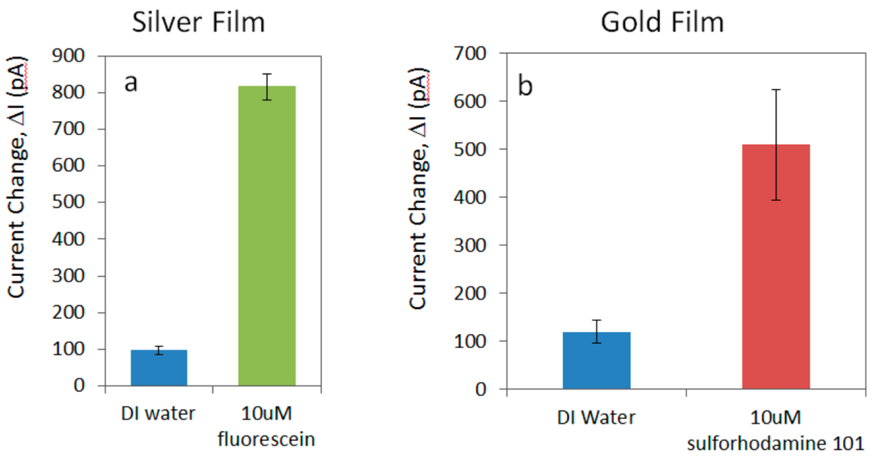

Figure 4. Current change, ΔI, with application of a 473 and 594 nm laser to a silver-island film (a) and a gold-island film (b), respectively. The current dramatically increases in the presence of the near-field fluorophores.

charging energies of 0.0032 and 0.056 eV for a single particle and for two particles on opposite sides of the film, respectively. These calculations serve to show that the charging energy required to transport an electron across the entire dry film (0.056 eV) is greater than $k_B T$ at room temperature (0.024 eV), preventing current flow across the film with zero applied voltage.

$C_{m,n}$ calculated above is the capacitance from a line of discrete nanoparticles in a large grid. However, the films are actually composed of many lines of nanoparticles, providing many starting and ending points for current flow across the film. $C_{m,n}$ may then be multiplied by the number of nanoparticle lines in the film, which is determined by the number of nanoparticles directly adjacent to the electrode surface and is calculated to be 7.57×10^4 nanoparticles directly adjacent to a 3.18 mm electrode surface. This leads to an overall theoretical film capacitance, C_{film}, of $\sim 1.08 \times 10^{-13}$ F. In addition to calculations, the film capacitance may also be evaluated experimentally through an applied voltage.[24,25]

Experimental $I-V$ (current vs voltage) curves for our silver and gold nanoparticle island films are shown in Figure 3. A columbic staircase is observed, which demonstrates an increased voltage to overcome the columbic blockade, increasing the electron transport rate between discrete metal particles, with similar trends also found elsewhere in the literature for metal nanoparticles.[22,25] From these curves the capacitance for the entire film may be experimentally determined, where,

$$C_{gate} = \frac{\Delta U}{\Delta Q} \tag{5}$$

where C_{gate} is the capacitance with an applied voltage, ΔU is the electrical charge in coulombs, and ΔQ is the potential in volts. ΔQ is the voltage required to induce one oscillation in Figure 3 below, as this is the potential required for electrons to "hop" across the film. This experimental value for capacitance of the silver film is found to be 2.8×10^{-13} F, which is in agreement with the theoretical value determined above for C_{film} of 1.08×10^{-13} F.

Upon application of a water solvent to the metal nanoparticles, the capacitance and charging energy required to move an electron across the 1 cm film are decreased according to eq 3, to 1.14×10^{-16} F and 0.0007 eV, respectively, allowing for increased electron transport between separate nanoparticles.

BACKGROUND SIGNAL

A deionized water solvent blank is first applied to the silver-island film, as shown in Figure 4a. The film is connected in circuit with a picoammeter, and a 473 nm *p*-polarized laser is applied to the surface. A detectable current increase is observed with laser application to the water solvent, representing a small background signal. This background signal is thought due to the excitation laser heating the system, raising $K_B T$, and increasing electron transport across the film. This background signal is evaluated experimentally by exposing the solvent covered metal surface to the excitation source in the absence of the fluorophore and measuring any current change. The fluorophore is then added into the system, and the excitation source is reapplied. The background current may then be subtracted from the fluorophore-induced current, where the overall current change due to excitation of the fluorophore solution on the metal surface may be represented by

$$\Delta I = I_{fluorophore} + I_{blank} \tag{6}$$

where ΔI is the current change with application of the excitation source, $I_{fluorophore}$ is the signal due to the fluorophore, and I_{blank} is the current change with laser application to the water solvent alone.

FLUOROPHORE-INDUCED PLASMON ELECTRICAL CURRENT IN METAL ISLAND FILMS (PC)

Fluorescein (10 μM) is added to the water solvent on the silver-island film, and the 473 nm *p*-polarized excitation laser is reapplied. A significant electrical current change is observed in the presence of the fluorophore (Figure 4a), well in excess of the background water signal. This current increase is thought due to energy transfer from the excited fluorophore to the silver islands, and subsequent electron transport between the islands. Fluorescein was chosen in this experiment due to the large overlap integral between its emission and the silver film plasmon absorbance. The same experiment was additionally performed on the gold-island film shown in Figure 2b, except that sulforhodamine 101 was chosen instead of fluorescein. Sulforhodamine 101 has a red-shifted emission as compared to fluorescein, increasing its overlap integral with the gold-island film. The current change with application of a 594 nm *p*-polarized excitation laser to the sulforhodamine 101 covered gold film is shown in Figure 4b.

With regard to fluorophore-induced plasmon resonance it is known that spherical metal nanoparticles much smaller than the wavelength of incoming light couple strongly with the far-field light.[4] Recent literature has demonstrated electrical current generation via the direct excitation of 3 nm gold nanoparticle plasmons with visible light.[34] However, as nanoparticle sizes grow toward the wavelength of incoming light, light scattering begins to dominate over absorption, and metal plasmons no longer couple strongly with direct light. However, a proximal fluorophore may still couple with and excite plasmons in larger size particles.[35] In other words, near-field coupling to a fluorophore is favored due to a wave vector mismatch between the far-field radiation and the metal particle.

Figure 5 depicts the irradiance of 5 μM fluorescein isothiocyanate on a silver-island film prepared via a liquid Tollens synthesis. The top panel of Figure 5 shows the electrical current on the dry film, where the charging energy is higher than the thermal energy at room temperature, and electron "hopping" is prevented. The middle and bottom panels show the induced electrical signal with irradiance of the water blank and fluorophore, respectively. This plot also demonstrates the ability of the current to be switched on and off (gated) with application of the irradiation source. It is worth noting the excitation light was manually "chopped" in the bottom two panels of Figure 5 to demonstrate that it is the excitation light and fluorophore combination only that induces the large plasmonic current.

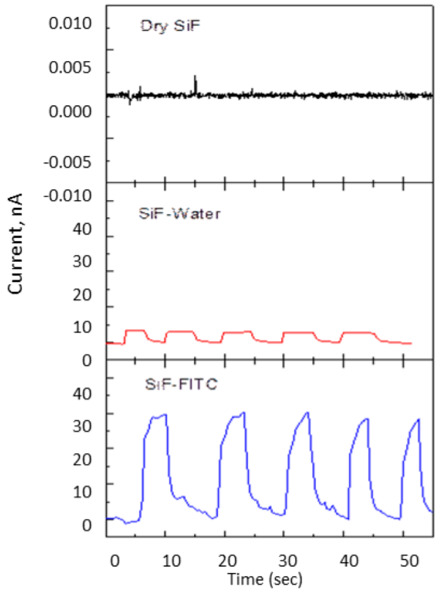

Figure 5. (Top) Electrical current through a dry noncontinuous silver island film. (Middle) Background current with irradiance of the water solvent. (Bottom) Current with 473 nm irradiance of 5 μM fluorescein isothiocyanate. The spikes in current are due to manual chopping of the excitation light, demonstrating that the current can be turned on and off by the application of light.

■ INDUCED PLASMON CURRENT DEPENDENCE ON FLUOROPHORE EXTINCTION COEFFICIENT

It is well-known that the magnitude of a fluorophores' extinction coefficient reflects both its oscillator strength and probability of excitation at a particular wavelength. Given that both Metal-Enhanced Fluorescence (MEF) and our novel plasmonic electricity phenomenon presented here involve a fluorophore-induced mirror dipole in the metallic films, we subsequently questioned the role of fluorophore extinction coefficient on the magnitude of the induced current. The extinction coefficient of sulforhodamine-101 was therefore measured at three different wavelengths, in essence, three different extinction coefficients and oscillator strengths of the same fluorophore, while keeping all other aspects of the experiment constant. The fluorophore-plasmon system was then excited at these wavelengths with a constant laser power, giving the electrical current as a function of sulforhodamine 101 extinction. The results demonstrate a clear upward trend in current generation as a function of extinction coefficient (Figure 6). The low extinction point of 1000 M^{-1} cm^{-1} serves as a control, demonstrating that when the molecule in the system is not excited, no significant system response is observed.

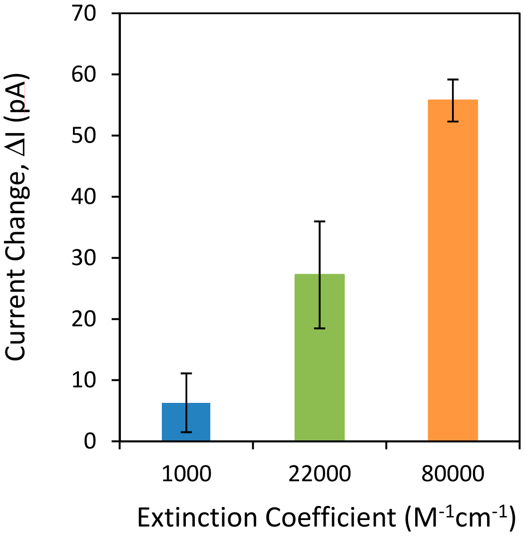

Figure 6. Observed current change upon laser excitation of sulforhodamine 101 as a function of its molecular extinction, at (blue) 473 nm, (green) 532 nm, and (orange) 594 nm. Each point is an average of three laser exposures and subsequent current measurements.

In addition to sulforhodamine 101, we also questioned how other fluorophores would indeed induce current (Figure 7). We have observed a linear relationship with fluorophore extinction coefficient, when all fluorphores were excited at the same laser power and fluorophore concentration. In addition, 40 nm sized colloidal gold particles were found to induce a significantly larger plasmonic current in the substrate as compared to any fluorophore. This observation is in complete agreement with our hypotheses that fluorphores with larger extinction coefficients induce larger currents, where 40 nm gold particles have extinction coefficients >10^6 M^{-1} cm^{-1}, 10× greater than typical xanthene type fluorophores.

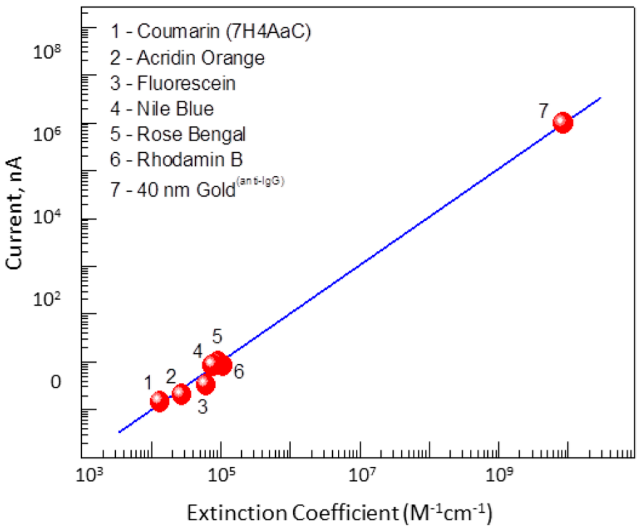

Figure 7. Dependence of plasmonic current generated in a silver island film on the extinction coefficient of several fluorophores.

DEPENDENCE OF THE INDUCED PLASMON CURRENT ON FLUOROPHORE CONCENTRATION

We subsequently questioned the role of fluorophore concentration on the magnitude of the induced current. Increasing the concentration of fluorophore on a metal film should provide more molecules with the proper proximity and orientation to the metal, allowing for an increased fluorophore-plasmon coupling, ultimately increasing the observed electrical current. Figure 8 shows the plasmonic current from a gold-island film as a function of sulforhodamine 101 concentration in deionized water. An upward trend is readily observed, linear within experimental error, indicating that an increase in the number of excited molecules on the metal film leads to greater electrical current generation. The minimum distinguishable analytical signal is taken as the sum of the mean solvent blank signal plus 3 times the standard deviation of multiple solvent blank measurements and is calculated to be 4.09×10^{-11} Amps. Sulforhodamine 101 is also an ideal fluorophore for investigation of the concentration effect on plasmonic current, because its presence does not exhibit a significant permittivity change with increasing concentration. For example, conductivities of 2 and 25 μM sulforhodamine 101 were measured to be 2.6 and 2.7 μS/cm, respectively. This is important because of the possibility that increasing the concentration of a charged fluorophore salt may alter the permittivity of solution between metal particles, potentially altering electron transport between particles in the metal film, i.e., increasing ε in eq 2.

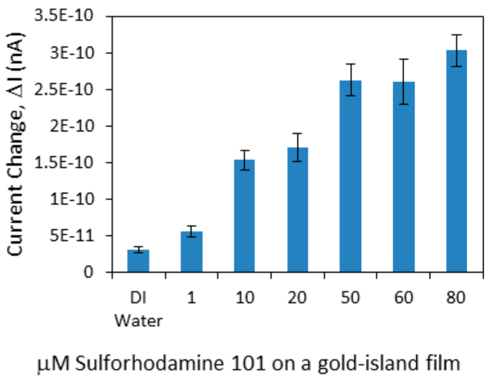

Figure 8. Fluorophore-induced electrical current on a gold-island film as a function of sulforhodamine 101 concentration in deionized water. Error bars are the mean of three measurements.

EFFECT OF EXCITATION LASER POLARIZATION ON THE MAGNITUDE OF FLUOROPHORE-INDUCED ELECTRICAL CURRENT

Finally, it is known that the excitation of surface plasmons in metal particle films is favored when fluorophore molecular dipoles are oriented perpendicular to the metal surface (p), as compared to parallel to the metal surface (s).[35] Surface plasmon resonance only occurs when excitation light is *p*-polarized, because in the *s* configuration the electric field is parallel to the surface causing the dipole to cancel out with its mirror image. This plasmon resonance excitation dependence on electric field orientation also extends to fluorophore-induced local excitation of plasmons.[35] In other words, fluorescent molecules with correct proximity, which are oriented perpendicular to the surface, preferentially couple to the metal, inducing plasmon resonance. The excitation laser was applied at a 45 deg angle to the metal surface, which allows for the electric component of the laser light to be oriented perpendicular to the metal surface in the *p*-configuration and parallel to the metal surface in the *s*-orientation. Fluorophores oriented perpendicular to the surface were preferentially excited with *p*-polarized laser light, and electrical current generation was subsequently studied. The polarization of the laser light was subsequently adjusted with a half wave plate, switching the electric field between *p* and *s* orientations (Figure 9). Our results demonstrate an increased current generation from *p*-polarized light, strongly supporting the hypothesis that coupling of *p*-oriented molecules is responsible for the observed system response (Figure 9). It is important to note that the fluorophores in this experiment are freely tumbling in solution. However, by choosing either *p* or *s* polarization, we are photoselecting those fluorophores whose dipoles are oriented either *p* or *s* to the surface.

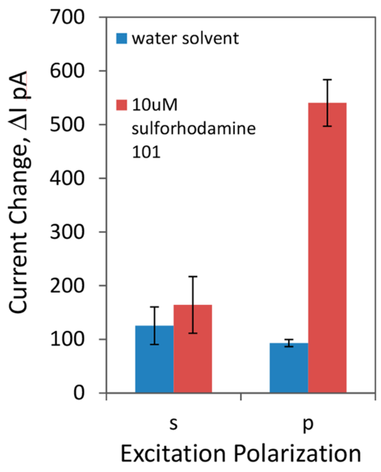

Figure 9. Current change as a function of excitation laser polarization direction with water (blue) and 10 μM sulforhodamine 101 (red), on a gold-island film. Error bars represent the mean of three measurements.

DOI: 10.1021/acs.jpcc.9b08249
J. Phys. Chem. C 2019, 123, 27770−27777

CONCLUSIONS

In conclusion, we have described a novel "plasmon to current" technique potentially capable of detecting fluorescence, without the need for a traditional photodetector and associated optics. This is thought to originate from energy transfer from proximal fluorescent molecules to closely spaced silver or gold nanoparticle islands, utilizing a similar mechanism as MEF.[7] In order to describe electron transport or "hopping" in our metal nanoparticle island films, we have determined the capacitance and charging energies of the films both theoretically with the concentric sphere model and experimentally, with results in good agreement with each other. Upon energy transfer from a proximal fluorophore, electron transport between individual metal particles is increased, resulting in the observed electrical current increase with application of a fluorophore excitation source. We have found this current to be dependent on the fluorophore extinction coefficient, providing a molecular fingerprint containing photophysical information, potentially allowing one to distinguish a specific fluorophore. In addition, this current is found dependent on the fluorophore concentration and excitation polarization. Finally, given the widespread use of fluorescence in the biosciences today, particularly for medical diagnostics,[36−38] we speculate that plasmonic current may significantly simplify detection platforms, Figure 10. Plasmonic current does not require a photodetector, and given that the magnitude of plasmonic current scales with the number of fluorophores in the near-field (i.e., close proximity to the metal), then our findings suggest a new approach to immunodiagnostics (Figure 10). This work is currently underway in our laboratory and will be reported in due course.

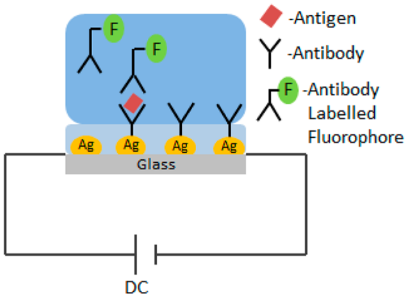

Figure 10. Cartoon depicting plasmonic electricity based immunodiagnostics.

MATERIALS AND METHODS

Materials. Silver nitrate (99.9%), sodium hydroxide (99.996%), ammonium hydroxide (30%), D-glucose, and silane-prep glass slides were obtained from Sigma-Aldrich. Silver and gold evaporation pellets (99.999%) were purchased from Research and PVD Materials Corporation and Kurt J. Lesker, respectively. Fluorophores purchased from Sigma-Aldrich include: fluorescein isothiocyante (FITC), coumarin (7H4AaC), acridin orange, fluorescein, Nile Blue, Rose Bengal, rhodamine B, and sulforhodamine 101.

Metal Island Film Preparation: Thermal Vapor Deposition. Silane-prep glass microscope slides (Sigma-Aldrich) were first cleaned with methanol, dried under dry N_2 and subsequently used as a substrate for silver and gold vapor deposition. Metal films were prepared with an Edwards BOC Auto 306 Vapor Deposition Unit, at a pressure of 9×10^{-6} Torr. The deposition rate was held constant at 0.1 Å/sond with deposition times ranging from 10 to 38 min. Prepared films were allowed to cool to room temperature and stored in a desiccator under vacuum until use.

Silver Island Film Preparation: Tollens Liquid Synthesis. A total of 200 μL of 1.25 M aqueous sodium hydroxide solution was added to 60 mL of 0.05 M aqueous silver nitrate, while stirring. Then 2 mL of ammonium hydroxide was then added in a dropwise fashion. The resulting solution was cooled to 5 °C, followed by placing silane-prep glass slides in the solution. Next, 15 mL of aqueous 0.27 M D-glucose solution was then added, and the mixture temperature was brought to 30 °C. The slide color was observed to turn green indicating particle formation, at which point the slides were removed from the solution, rinsed in deionized water, and stored in a desiccator under vacuum.

Instrumentation. Absorption spectra of prepared silver and gold films were collected using a single beam Varian Cary 50-Bio UV−vis spectrophotometer. Electrical current through the system was measured with a Keithley 6487 picoammeter/voltage source, in either an open circuit configuration or under an applied potential, with digital output to an external computer. Electrode materials were selected to match the metal nanoparticle film (for example silver-on-silver). The electrodes were positioned to make simultaneous contact with the metal nanoparticle film and the liquid solvent. Scanning electron microscopy of vapor deposited films was performed using a Nova NanoSEM 450 with secondary electron imaging.

Plasmonic Current Measurements. Fluorophore solutions were prepared in deionized water, pipetted onto electrically noncontinuous metal island films, and allowed to diffuse into the gaps between separate nanoparticle islands. Upon addition of solution to the metal, electrical current due to convection was allowed to stabilize for approximately 5 min. Fluorophores were then excited either with a Xe-Arc lamp or a *p*-polarized LaserMate 473 nm continuous wave laser directed at the film surface, with the excitation power adjusted using an absorbing neutral-density filter wheel (Edmund Optics; Supporting Information, Figure S3). Positioning of the laser across the substrate was adjusted manually in 2 mm increments. Change in electrical current through the fluorophore−metal system was monitored in an open circuit configuration or under an applied potential at room temperature (20 °C) and reported as the absolute value of current change, ΔI, with application of the excitation source. Laser output polarization was adjusted with a half-wave plate (Special Optics Inc.).

ASSOCIATED CONTENT

Ⓢ Supporting Information

The Supporting Information is available free of charge on the ACS Publications website at DOI: 10.1021/acs.jpcc.9b08249.

> Absorption spectra of silver and gold films prepared over a range of thermal vapor deposition times are displayed in Figure S1. The derivation of the model for calculation of the capacitance of a metal nanoparticle island film is displayed in Figure S2. A schematic of the experimental setup is shown in Figure S3. (PDF)

AUTHOR INFORMATION

Corresponding Author

*All Geddes@umbc.edu.

ORCID

Joshua Moskowitz: 0000-0002-4768-9082

Notes

The authors declare no competing financial interest.

■ ACKNOWLEDGMENTS

The authors would like to thank the Institute of Fluorescence as well as the Department of Chemistry and Biochemistry at the University of Maryland Baltimore County (UMBC) for financial support. Also a special thanks to the UMBC Nanoimaging Facility for the imaging used in this work.

■ REFERENCES

(1) Lakowicz, J. R. *Principles of Fluorescence Spectroscopy*, 3rd ed.; Springer: New York, 2006; pp 841−867.

(2) Geddes, C. D.; Lakowicz, J. R. Metal-Enhanced Fluorescence. *J. Fluoresc.* **2002**, *12*, 121−129.

(3) Eustis, S.; El-Sayed, M. Aspect Ratio Dependence of the Enhanced Fluorescence Intensity of Gold Nanorods: Experimental And Simulation Study. *J. Phys. Chem. B* **2005**, *109* (34), 16350−16356.

(4) Pelton, M.; Bryant, G. W. *Introduction to metal-nanoparticle plasmonics*; Wiley: Hoboken, NJ, 2013.

(5) Li, J.; Krasavin, A. V.; Webster, L.; Segovia, P.; Zayats, A. V.; Richards, D. Spectral Variation of Fluorescence Lifetime Near Single Metal Nanoparticles. *Sci. Rep.* **2016**, *6*, 21349.

(6) Weitz, D. A.; Garoff, S.; Hanson, C. D.; Gramila, T. J.; Gersten, J. I. Fluorescent Lifetimes Of Molecules on Silver-Island Films. *Opt. Lett.* **1982**, *7* (2), 89−91.

(7) Geddes, C. D. *Metal-Enhanced Fluorescence*; Wiley: Hoboken, NJ, 2010; pp 1−20.

(8) Zhang, Y.; Dragan, A.; Geddes, C. D. Wavelength Dependence of Metal-Enhanced Fluorescence. *J. Phys. Chem. C* **2009**, *113* (28), 12095−12100.

(9) Novotny, L.; van Hulst, N. Antennas For Light. *Nat. Photonics* **2011**, *5* (2), 83−90.

(10) Yongxia, Z.; Aslan, K.; Previte, M. J. R.; Geddes, C. D. Metal-Enhanced E- Type Fluorescence. *Appl. Phys. Lett.* **2008**, *92* (1), 013905.

(11) Gupta, R.; Dyer, M. J.; Weimer, W. A. Preparation and Characterization of Surface Plasmon Resonance Tunable Gold And Silver Films. *J. Appl. Phys.* **2002**, *92* (9), 5264−5271.

(12) Homola, J.; Piliarik, M. Surface Plasmon Resonance Based Sensors. *Springer Series on Chemical Sensors and Biosensors*; Springer: Berlin, 2006.

(13) Wei, W.; Zhang, X.; Ren, X. Plasmonic Circular Resonators for Refractive Index Sensors and Filters. *Nanoscale Res. Lett.* **2015**, *10*, 211−211.

(14) Skoog, D. A.; West, D. M. *Principles of instrumental analysis*; Rinehart and Winston: New York, 2010.

(15) Jeanmaire, D. L.; Van Duyne, R. P. Surface Raman Spectroelectrochemistry. Part I. Heterocyclic, Aromatic, And Aliphatic Amines Adsorbed On The Anodized Silver Electrode. *J. Electroanal. Chem. Interfacial Electrochem.* **1977**, *84*, 1−20.

(16) Le Ru, E. C.; Blackie, E.; Meyer, M.; Etchegoin, P. G. Surface Enhanced Raman Scattering Enhancement Factors: A Comprehensive Study. *J. Phys. Chem. C* **2007**, *111* (37), 13794−13803.

(17) Kawata, S.; Inouye, Y.; Verma, P. Plasmonics for near-field nano-imaging and superlensing. *Nat. Photonics* **2009**, *3*, 388−394.

(18) Gotte, J. Principles of Nano-Optics, 2nd ed., by Lukas Novotny and Bert Hecht. *Contemp. Phys.* **2013**, *54* (2), 123−124.

(19) Tang, L.; Kocabas, S. E.; Latif, S.; Okyay, A. K.; Ly-Gagnon, D. S.; Saraswat, K. C.; Miller, D. A. Nanometre-Scale Germanium Photodetector Enhanced By A Near-Infrared Dipole Antenna. *Nat. Photonics* **2008**, *2* (4), 226−229.

(20) Falk, A. L.; Koppens, F. L.; Yu, C. L.; Kibum, K.; de Leon Snapp, N.; Akimov, A. V.; Hongkun, P. Near-Field Electrical Detection of Optical Plasmons and Single-Plasmon Sources. *Nat. Phys.* **2009**, *5* (7), 475−479.

(21) Moore, R. G. C.; Evans, S. D.; Shen, T.; Hodson, C. E. C. Room-Temperature Single-Electron Tunnelling In Surfactant Stabilised Iron Oxide Nanoparticles. *Phys. E* **2001**, *9* (2), 253−261.

(22) Schmid, G. D. *Nanoparticles: From Theory to Application*; Wiley-VCH: Weinheim, Germany, 2004.

(23) Markovich, G.; Collier, C. P.; Heath, J. R. Reversible Metal-Insulator Transition In Ordered Metal Nanocrystal Monolayers Observed By Impedance Spectroscopy. *Phys. Rev. Lett.* **1998**, *80* (17), 3807−3810.

(24) Kano, S.; Tanaka, D.; Sakamoto, M.; Teranishi, T.; Majima, Y. Control of Charging Energy In Chemically Assembled Nanoparticle Single-Electron Transistors. *Nanotechnology* **2015**, *26* (4), 045702−045702.

(25) Negishi, R.; Hasegawa, T.; Tanaka, H.; Terabe, K.; Ozawa, H.; Ogawa, T.; Aono, M. Size-Dependent Single Electron Tunneling Effect In Au Nanoparticles. *Surf. Sci.* **2007**, *601*, 3907−3911.

(26) Weaver, M. J.; Gao, X. Molecular Capacitance: Sequential Electron-Transfer Energetics For Solution-Phase Metallic Clusters In Relation To Gas-Phase Clusters And Analogous Interfaces. *J. Phys. Chem.* **1993**, *97* (2), 332−332.

(27) Garcia-Morales, V.; Mafe, S. Monolayer-Protected Metallic Nanoparticles: Limitations of The Concentric Sphere Capacitor Model. *J. Phys. Chem. C* **2007**, *111* (20), 7242−7250.

(28) Di, L.; Jinghong, L. Preparation, Characterization And Quantized Capacitance Of 3-Mercapto-1,2-Propanediol Monolayer Protected Gold Nanoparticles. *Chem. Phys. Lett.* **2003**, *372* (5), 668−673.

(29) Wolfe, R. L.; Murray, R. W. Analytical Evidence For The Monolayer-Protected Cluster Au225[(S(CH2)5CH3)]75. *Anal. Chem.* **2006**, *78* (4), 1167−1173.

(30) Saito, Y.; Wang, J. J.; Smith, D. A.; Batchelder, D. N. A Simple Chemical Method for The Preparation Of Silver Surfaces For Efficient SERS. *Langmuir* **2002**, *18*, 2959−2961.

(31) Rycenga, M.; Cobley, C. M.; Jie, Z.; Weiyang, L.; Moran, C. H.; Qiang, Z.; Dong, Q.; Younan, X. Controlling The Synthesis And Assembly Of Silver Nanostructures for Plasmonic Applications. *Chem. Rev.* **2011**, *111* (6), 3669−3712.

(32) Pribik, R.; Dragan, A. I.; Zhang, Y.; Gaydos, C.; Geddes, C. D. Metal-enhanced fluorescence (MEF): physical characterization of Silver-island films and exploring sample geometries. *Chem. Phys. Lett.* **2009**, *478* (1), 70−74.

(33) Asad, J. H.; Hijjawi, R. S.; Sakaji, A.; Khalifeh, J. M. Capacitance Between Two Points On An Infinite Grid. *Eur. Phys. J.: Appl. Phys.* **2005**, *32* (3), 149−154.

(34) Han, X.; Shokri Kojori, H.; Leblanc, R. M.; Kim, S. J. Ultrasensitive Plasmonic Biosensors for Real-Time Parallel Detection Of Alpha-L-Fucosidase And Cardiac-Troponin-I In Whole Human Blood. *Anal. Chem.* **2018**, *90* (13), 7795−7799.

(35) Lakowicz, J. R. Radiative Decay Engineering 3. Surface Plasmon-Coupled Directional Emission. *Anal. Biochem.* **2004**, *324*, 153−169.

(36) Melendez, J. H.; Huppert, J. S.; Jett-Goheen, M.; Hesse, E. A.; Quinn, N.; Gaydos, C. A.; Geddes, C. D. Blind Evaluation of The Microwave-Accelerated Metal-Enhanced Fluorescence Ultrarapid And Sensitive Chlamydia Trachomatis Test By Use Of Clinical Samples. *Journal of Clinical Microbiology.* **2013**, *51* (9), 2913−2920.

(37) Zhang, Y.; Agreda, P.; Kelly, S.; Gaydos, C.; Geddes, C. D. Development Of A Microwave-Accelerated Metal-Enhanced Fluorescence 40 Seconds, < 100 Cfu/Ml Point Of Care Assay For The Detection Of Chlamydia Trachomatis. *IEEE Trans. Biomed. Eng.* **2011**, *58* (3), 781−784.

(38) Melendez, J. H.; Santaus, T.; Brinsley, G.; Kiang, D.; Mali, B.; Hardick, J.; Gaydos, C. A.; Geddes, C. D. Microwave-Accelerated Method For Ultra-Rapid Extraction Of Neisseria Gonorrhoeae DNA For Downstream Detection. *Anal. Biochem.* **2016**, *510*, 33−40.

DOI: 10.1021/acs.jpcc.9b08249